Temperature and Isotope Dependence of the Reaction of Methyl Radicals with Deuterium Atoms

Paul W. Seakins,* Struan H. Robertson,† and Michael J. Pilling

School of Chemistry, University of Leeds, Leeds LS2 9JT, U.K.

David M. Wardlaw

Department of Chemistry, Queen's University, Kingston, Ontario K7L 3N6, Canada

Fred L. Nesbitt, R. Peyton Thorn, Walter A. Payne, and Louis J. Stief*

Laboratory for Extraterrestrial Physics, NASA Goddard Space Flight Center, Greenbelt, Maryland 20771

Received: June 23, 1997; In Final Form: October 13, 1997[⊗]

The reactions of methyl isotopomers (CH_3, CH_2D, and CHD_2) with excess deuterium atoms have been studied using discharge flow/mass spectrometry at 298 K and at pressures of ∼1 Torr (helium). At these low pressures the initially formed methane complex is not stabilized. However, zero-point energy differences between methyl isotopomers mean that ejection of H from energized methane is favored. In consequence, regeneration of the reactant isotopomer is inefficient and values of k_{1a-c} may be extracted from the appropriate methyl radical decay. The experimental values can be used to calculate the high-pressure values for each isotopic reaction: (1a) $CH_3 + D \rightarrow CH_2D + H$, $k_{1a}^{\infty} = (2.3 \pm 0.6) \times 10^{-10}$ cm^3 molecule^{-1} s^{-1}; (1b) $CH_2D + D \rightarrow CHD_2 + H$, $k_{1b}^{\infty} = (2.1 \pm 0.5) \times 10^{-10}$ cm^3 molecule^{-1} s^{-1}; (1c) $CHD_2 + D \rightarrow CD_3 + H$, $k_{1c}^{\infty} = (1.9 \pm 0.5) \times 10^{-10}$ cm^3 molecule^{-1} s^{-1}. These, in turn, can be corrected for isotopic substitution and averaged to give a value of $(2.9 \pm 0.7) \times 10^{-10}$ cm^3 molecule^{-1} s^{-1} for the limiting high-pressure recombination rate coefficient of CH_3 and H. The errors of ∼25% are estimates of both the statistical and systematic errors in the measurements and calculations. The results are in agreement with an earlier direct determination of reaction 1a and recent theoretical calculations. The previous direct studies of $CH_3 + H$ in the fall off region have been reanalyzed using master equation techniques and are now shown to be in good agreement with current experimental and theoretical calculations. Reaction 1c was also studied at 200 K, with k_{1c} falling by approximately 35% from its room-temperature value, confirming theoretical predictions of a positive temperature dependence for the high-pressure limiting rate coefficient for the reaction $CH_3 + H + M \rightarrow CH_4 + M$.

I. Introduction

Radical−radical and radical-atom reactions play important roles in a variety of chemical systems including combustion[1,2] and planetary atmospheres.[3] Occurring as they do on Type II potential energy surfaces with no maxima and hence no well-defined transition states, these reactions provide stringent tests of theoretical models. One of the most successful of these models is the flexible transition-state theory (FTST), based on a variational approach introduced by Marcus and Wardlaw that predicts negative temperature dependencies for radical−radical reactions, such as $CH_3 + CH_3$, but a slight positive temperature dependence for the reaction of methyl radicals and atomic hydrogen.[4]

$$CH_3 + H + M \rightarrow CH_4 + M \qquad \text{(R1)}$$

This reaction is important in models for both high-temperature combustion chemistry and the low-temperature atmospheric chemistry of the giant planets.

The reaction of methyl radicals with atomic hydrogen is a pressure-dependent recombination process which can be represented as a sequence of elementary reactions:

$$CH_3 + H \leftrightarrow [CH_4]^* \qquad \text{(R1f,1r)}$$

$$[CH_4]^* + M \rightarrow CH_4 + M \qquad \text{(R1s)}$$

An energized methane molecule, $[CH_4]^*$, is formed on the combination of CH_3 and H (R1f). The short-lived complex that is formed can either redissociate (R1r) or be collisionally stabilized (R1s) by a bath gas, M. The dependence on [M] means that the overall reaction is generally pressure dependent; however, at high pressures, $k_{1s}[M] \gg k_{1r}$ and the overall rate coefficient for methyl radical removal, k_1^{∞}, becomes pressure independent. The relatively small number of vibrational modes in the excited methane molecule means that its lifetime before redissociation ($1/k_{1r}$) is very short, and under conventional laboratory conditions the reaction is well into the fall off region making comparisons with the FTST calculations of k_1^{∞} difficult.

Reaction 1 plays a vital role in combustion chemistry, the importance of the reaction being emphasized by a recent sensitivity analysis on the combustion of methane. In this study[5] the sensitivity of the flame velocity to the rate coefficients of the methane model (Leeds methane oxidation model) were investigated at a variety of equivalence ratios using "Premix" the one-dimensional flame simulation program from the CHEMKIN package.[6] Even for a fuel-rich mixture (equivalence ratio 0.6), reaction 1 was the sixth most sensitive reaction, while for stoichiometric or lean conditions (equivalence ratio 1.3)

† Present address: Molecular Simulations Inc., 240/250 The Quorum, Barnwell Rd, Cambridge CB5 8RE, U.K.

⊗ Abstract published in *Advance ACS Abstracts,* December 1, 1997.

S1089-5639(97)02034-3 CCC: $14.00

reaction 1 was the second most important reaction, behind only the chain branching reaction of hydrogen atoms with molecular oxygen.

Values for k_1^0 and k_1^∞ at lower temperatures are needed for models[7] of the atmospheres of the giant planets Jupiter and Saturn. Even though the high-pressure limit is not approached in these atmospheric systems, the pressure ranges involved are such that an analytical expression involving k_1^0 and k_1^∞ is needed as a model input to generate rate coefficient values as a function of altitude.

A majority of the previous determinations of the rate coefficient for reaction 1 have been indirect studies,[8−10] monitoring the methane production at low pressures from the following sequence of reactions:

$$H + C_2H_4 + M \rightarrow C_2H_5 + M \qquad (R2)$$

$$C_2H_5 + H \rightarrow 2CH_3 \qquad (R3)$$

$$CH_3 + H + M \rightarrow CH_4 + M \qquad (R1)$$

Higher pressure (>100 Torr) studies have been initiated by the Hg photosensitization of ethane,[11] flash photolysis of azomethane/ethene mixtures,[12,13] or methane/water mixtures.[14] The reaction compositions have been monitored by gas chromatographic end product analysis or mass spectrometry, an exception being the work of Sworski et al.[14] who monitored the reaction in real time using kinetic absorption spectroscopy of methyl radicals at 216 nm. The data from these various determinations are widely scattered, and long extrapolations are required to predict k_1^∞.

The most recent and direct study is discussed in some detail below as it forms the basis of the work to be described in this paper and raises a number of important questions. Brouard et al.[15−17] monitored reaction 1 in real time following the photolysis of acetone at 193 nm. The photolysis generates an excess of methyl radicals with a minor channel of the photolysis producing H atoms. H atoms were removed by reaction 1, which proceeds in competition with the recombination of methyl radicals (R4).

$$CH_3 + CH_3 + M \rightarrow C_2H_6 + M \qquad (R4)$$

The concentrations were such that the decay of CH_3 was determined by reaction 4. The decay of H was monitored by resonance fluorescence while absolute methyl radical concentrations were obtained by kinetic absorption spectroscopy (at 216 nm) combined with the well-determined value of the absorption cross section at this wavelength.[18] Under these conditions there is an analytical solution for the decay of H atoms which depends on k_1, the zero-time concentration of CH_3, k_4, and first-order loss processes for H. Using experimentally determined values of the H atom diffusion rate and direct measurements of k_4 from simultaneous measurements of [CH_3] (t), the overall rate coefficient for reaction 1 was determined between 300 and 600 K and 25 and 600 Torr.

Even at the lowest temperatures and highest pressures of the study (300 K, 600 Torr) the reaction is still far from the high-pressure limit (k_1^∞) which Brouard et al.[15] estimated by both Troe factorization methods and RRKM/master equation calculations. However, Brouard et al.[15] recognized that k_1^∞ could also be obtained from the isotopic substitution of H with D. They argued that the difference in zero-point energies in the CH_3 and CH_2D radicals ensures that, in the scheme outlined below, k_{1r} is always very much less than k_d, and therefore once the energized methane is formed it either dissociates into CH_2D + H or is stabilized to CH_3D. The validity of this assumption is discussed further in section IV. Monitoring the rate of removal of D atoms therefore gives a direct measure of k_{1a} for the partially deuterated system, and the appropriate isotopic correction (section V) should give the high-pressure limit for the methyl + H reaction.

$$\begin{array}{ccc} & k_{1f} \quad\quad k_d & \\ CH_3 + D \Leftrightarrow & CH_3D^* & \rightarrow CH_2D + H \\ & k_{1r} \quad \downarrow + [M]\, k_{1s} & \\ & CH_3D & \end{array}$$

For these experiments D atoms had to be generated from an alternative source; the photolysis of N_2O/D_2 mixtures and k_{1a} extracted from numerical fitting of the resultant decay curves although the D and CH_3 profiles were still dominated by reactions 1 and 4, respectively. The added complexity of this system could lead to uncertainties in the estimate of k_{1a}. The system was studied over the pressure and temperature ranges $50 < p$ (Torr) < 600 and $289 < T$ (K) < 401, and the observed rate coefficient was found to be invariant over these conditions.

The level of agreement between theoretical extrapolations of the CH_3 + H data and the direct estimation via the deuterated substitution was not good, with a difference of over a factor of 2.[15] For example at 300 K, extrapolation of the CH_3 + H data lead to a high-pressure limiting rate coefficient of 4.7×10^{-10} cm^3 molecule^{-1} s^{-1} , whereas a value of $(2.26 \pm 0.19) \times 10^{-10}$ cm^3 molecule^{-1} s^{-1} was calculated from the CH_3 + D data after isotopic correction. Three possible explanations can be proposed to explain the disagreement: (1) errors in one or both of the experimental determinations, (2) errors in the extrapolation methods used to determine k_1^∞, (3) an abnormal isotope effect such that simple corrections cannot be made between the fully hydrogenated and partially deuterated systems.

This paper describes a discharge flow/mass spectrometric determination of k_1^∞ at 300 and 200 K. For experimental reasons (section II) a range of methyl isotope (CH_3, CH_2D, and CHD_2) reactions with D atoms were studied:

$$CH_3 + D \rightarrow CH_2D + H \qquad (R1a)$$

$$CH_2D + D \rightarrow CHD_2 + H \qquad (R1b)$$

$$CHD_2 + D \rightarrow CD_3 + H \qquad (R1c)$$

However, in each case the principles are similar to those used in the work of Brouard et al.[15] The sensitivity of the mass spectrometric monitoring system allows the reaction to be followed with an excess of D atoms, minimizing the effects of methyl radical recombination. The aims of the investigation are to determine the nature of the temperature dependence of k_1^∞ and seek to answer some of the questions raised by Brouard et al.[15] In addition, we have also tried to refit the CH_3 + H pressure- and temperature-dependent data of Brouard et al. to take advantage of recently calculated microcanonical rate coefficients for methane dissociation and developments in software for analyzing pressure-dependent reactions.

The layout of the paper is as follows: Section II describes the experimental technique used. Section III describes the initial results, the kinetic scheme used to extract k_{1a-c}, and the calculation of diffusional corrections. The justification of the isotope experiments is addressed in section IV, and the method for accounting for isotopic substitution is presented in section V. The reevaluation of the CH_3 + H data is contained in section VI and, finally, the results are reviewed in section VII.

II. Experimental Section

II.a. Discharge Flow Reactor. All experiments were performed in a Pyrex flow tube, ~60 cm long and 28 mm in diameter, the inner surface of the tube being lined with Teflon. A majority of experiments were performed at ambient temperatures (294−298 K); a series of low-temperature (200 K) measurements were made by circulating ethanol from a cooled reservoir through a jacket surrounding the flow tube. The flow tube was coupled via a two-stage stainless steel collision-free sampling system to a quadrupole mass spectrometer (Extrel, Inc.). The system has been described in detail in previous publications.[19,20]

Helium carrier gas was flowed at rates between 400 and 600 sccm into the flow tube. The linear flow velocity ranged from 2000 to 2500 cm s^{-1} at nominal pressures in the region of 1 Torr (133 Pa). In calculating the linear flow velocity, the plug flow assumption was made. The flow velocity is calculated from the gas constant, temperature, cross-sectional area of the flow tube, total gas flow, and total pressure. Gas flows were measured and controlled by electronic flow meters (MKS) suitably calibrated for the gas mixes flowing through them. Deuterium and the appropriate methane isotope were premixed and then introduced into the flow tube via a Pyrex moveable injector, the position of which could be changed from a distance between 2 and 40 cm from the sampling point. A sidearm, at the upstream end of the flow tube, contained a microwave discharge for the production of F atoms.

II.b. Radical Generation and Monitoring. Fluorine atoms were produced at the upstream end of the flow reactor by passing molecular F_2 (5% in helium) through a microwave discharge (~50 W, 2450 MHz). The discharge region consisted of a 3/8 in. ceramic tube mounted inside the discharge arm. About 40−60% of the F_2 was dissociated, and therefore a significant concentration of F_2 entered the flow tube. The effect of F_2 on the kinetics of the methyl radical consumption was accounted for in the numerical analysis.

At the tip of the sliding injector both D atoms and the desired methyl isotopomers were produced simultaneously via the following reactions:

$$F + D_2 \rightarrow DF + D \quad \text{(ref 21)} \qquad \text{(R5)}$$

$$F + CH_4 \rightarrow HF + CH_3 \quad \text{(ref 22)} \qquad \text{(R6a)}$$

$$F + CH_3D \rightarrow HF + CH_2D \qquad \text{(R6b)}$$

$$F + CHD_3 \rightarrow DF + CHD_2 \qquad \text{(R6c)}$$

Concentrations of D_2 were in the region of $2.5-6.5 \times 10^{14}$ molecules cm^{-3} to ensure rapid conversion of F atoms to D atoms or methyl radicals. The ratio of methane:D_2 was adjusted to vary the radical-to-atom ratio.

Methyl radicals were detected at the appropriate mass following low-energy electron ionization, to minimize the background signal from methane or hydrocarbon impurity fragmentation. A careful search was undertaken to optimize ionization conditions for maximum signal to background, while still retaining an appreciable signal level. The signal-to-background ratio decreased with increasing electron energy and ion current, even for nominal electron energies significantly below the threshold energy for methane fragmentation. Optimum conditions were found to be 11.5 eV electron energy and 0.2 mA ion current. Mass scans were recorded for the region $m/z = 15-18$, and signals were taken as the integrated area of the appropriate mass peak. Signals were typically averaged for 30−60 s for each injector position. The background signal showed some variability and was significantly reduced by the use of a cold shroud (77 K) in the inner chamber. Background signals for masses 16 (CH_2D) and 17 (CHD_2) were significantly lower than for mass 15 (CH_3).

A few experiments were undertaken using CH_2DI as a source of methyl radicals. The reaction of F atoms with CH_2DI should, by analogy with the reaction with methyl iodide,[23]

$$F + CH_3I \rightarrow IF + CH_3 \quad (70\%)$$

$$F + CH_3I \rightarrow HF + CH_2I \quad (30\%)$$

yield predominantly CH_2D with the minor channels producing noninterfering radicals and with the mass of the parent compound being well separated from product methyl radicals. This is not the case in studying, for example, the reaction of CH_2D generated from CH_2D_2 where there are significant interferences at mass 17 from the concurrently generated CHD_2 and mass 18 from the parent methane. Unfortunately significant parent fragmentation of the iodide occurs giving methyl ions, even at low (10.5 eV) electron energies, and there is little improvement in the signal-to-background ratio.

II.c. Titrations. Absolute F atom concentrations were determined by the fast titration reactions

$$F + Cl_2 \rightarrow Cl + ClF \qquad \text{(R7)}$$

$$k_7(T = 298\ \text{K}) = 1.60 \times 10^{-10}\ \text{cm}^3\ \text{molecule}^{-1}\ \text{s}^{-1}\ [24]$$

or

$$F + CH_4 \rightarrow HF + CH_3 \qquad \text{(R6a)}$$

$$k_{6a}(T = 298\ \text{K}) = 7.84 \times 10^{-11}\ \text{cm}^3\ \text{molecule}^{-1}\ \text{s}^{-1}\ [22]$$

The F atom concentration was determined (±6% experimental error) by measuring the decrease in the Cl_2 (CH_4) signal when the discharge was initiated. The absolute F concentration is given by $[F] = [Cl_2]_{\text{disc off}} - [Cl_2]_{\text{disc on}}$. As discussed previously for N atoms studies,[25] a number of precautions were taken in order to avoid systematic errors in this type of measurement.

A series of experiments was also performed to verify the conversion of F → D and to ensure that the concentration of D atoms remained uniform along the flow tube. In this case the titration reaction was with Br_2.

$$D + Br_2 \rightarrow DBr + Br \qquad \text{(R8)}$$

$$k_8(T = 298\ \text{K}) = 5.6 \times 10^{-11}\ \text{cm}^3\ \text{molecule}^{-1}\ \text{s}^{-1}\ [26]$$

Bromine was introduced at a fixed inlet 47 cm from the discharge and 13 cm before the sampling point, with a residence time and concentration in the flow tube large enough to ensure complete conversion of D to Br before sampling. Titrations were repeated with the D_2 injector at a number of positions, thus giving the D atoms a range of residence times in the flow tube before reacting with Br_2. In all cases the concentrations of D atoms were constant within the experimental error of the determinations (±5%) and equal (within the combined experimental error of ±11%) to [F] as determined by titration with CH_4.

II.d. Materials. Helium (99.999%, Air Products) was dried by passage through a trap held at liquid nitrogen temperature before entering the flow system. F_2 (99.9%, Cryogenic Rare Gases, 5% in He), H_2 (99.999%, Air Products UHP), D_2 (99.5%,

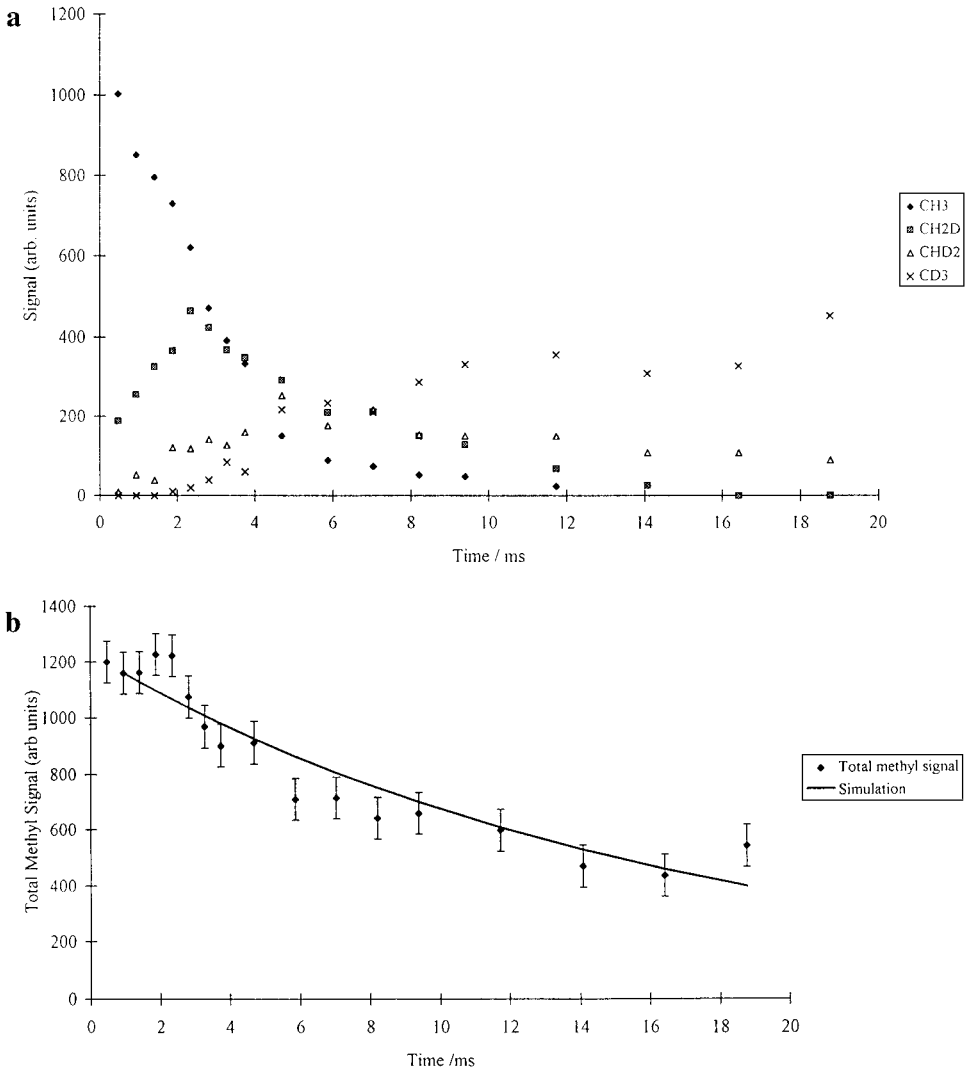

Figure 1. (a) Plot showing the gradual conversion of $CH_3 \rightarrow CD_3$ following the initial production of CH_3 and D. The growth and decay of the CH_2D and CHD_2 intermediates can clearly be seen. (b) Plot of the total methyl signal (i.e., the sum of the CH_3, CH_2D, CHD_2, and CD_3 signals). The solid line is the expected decay due to wall loss and methyl recombination.

Air Products), Cl_2 (99.9%, Matheson, 3.5% in He), CH_4 (99.9995% M. G. Industries), CH_3D, CHD_3, and CH_2D_2 (MSD Isotopes, 98.9 atom % D) were used as provided without further purification.

III. Results

III.a. Initial Results. Figure 1a shows the temporal profile of each of the methyl radicals (CH_3, CH_2D, CHD_2, and CD_3) following the initial production of CH_3 radicals via reaction 6. The sequential deuteration of the methyl radicals as each of the H atoms is replaced by deuterium can readily be seen.

$$\begin{array}{ccccccc} & +D & & +D & & +D & \\ CH_3 & \rightarrow & CH_2D & \rightarrow & CHD_2 & \rightarrow & CD_3 \\ & -H & & -H & & -H & \end{array}$$

Summation of the total methyl radical signal gives the temporal profile shown in Figure 1b. The total methyl signal is, as expected, decaying with a similar time constant to that observed for the decay of methyl radicals in the presence of similar quantities of H atoms, where methyl radicals are slowly removed by recombination to form ethane or by loss at the wall. The solid line in Figure 1b is a simulation based on experimental conditions and literature values for methyl recombination rate[27] coefficients as no experiments were performed with identical initial methyl radical concentrations. At these pressures, the reaction with deuterium atoms is merely changing the isotopic composition of the methyl radicals; it does not increase the overall rate of removal of methyl radicals. Monitoring and calibration of the peak at $m/z = 30$ (ethane) indicates that under typical conditions of the experiment ($[CH_3]_0 < 5 \times 10^{11}$ molecules cm^{-3}, $[D]_0$:$[CH_3]_0 > 20$:1) less than 5% of the methyl radicals are removed as ethane.

III.b. Data Analysis. Signals for a single methyl isotopomer at the appropriate m/z ratio were averaged for 30−60 s per injector position. Background signals were taken at the beginning and end of each decay by moving the injector to a distance, typically 40 cm (∼20 ms), such that all of the methyl radicals under study had been consumed by the reaction with D atoms. For most analyses a simple average of the two background levels was subtracted from each datum point to give the net methyl signal. In some instances a larger drift in background signal was observed. In these cases a variable background subtraction was used, the actual value subtracted being the appropriate time-weighted interpolation between the initial and final background readings. A typical decay trace is shown in Figure 2. Unfortunately higher concentrations of methyl radicals, which would have reduced the significance of background signals, could not be used. The higher concentration of D atoms, required to

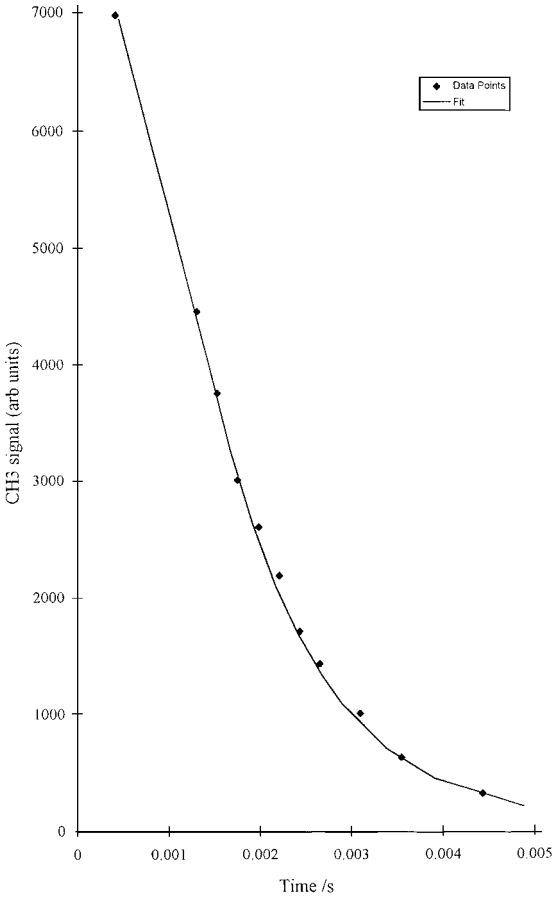

Figure 2. Typical CH_3 + D decay curve (◆) with the numerical fit to the data (solid line).

ensure that reactions 1a−c were isolated, would have resulted in pseudo-first-order rate coefficients faster than can be measured with the present apparatus.

Experimental conditions were chosen so that D atoms were always in excess; however, numerical simulations showed that, under the conditions that could be used, the experimentally observed decays, while being approximately exponential in nature, were not simple processes but involved contributions at the beginning of the decay from the generation of D and methyl radicals via reactions 5 and 6, and toward the end of the decay, from a small regeneration of methyl radicals via the sequence of reactions:

$$D + F_2 \rightarrow DF + F \qquad (R9)$$

$$F + D_2 \rightarrow DF + D \qquad (R5)$$

$$F + \text{methane} \rightarrow \text{methyl} + HF \qquad (R6)$$

Under these conditions k_{1a-c} can only be extracted by numerical simulations, and the mechanisms used for analysis are presented in Table 1. There are two complicating factors for the analysis: diffusional corrections and wall reactions.

Diffusional Corrections. In a discharge flow experiment distance measurements are converted to time using the relationship

$$\text{time } (t) = \text{distance } (x)/\text{velocity } (v) \qquad (E1)$$

where velocity is the linear flow velocity (v_{lin}) plus the diffusional term due to the concentration gradient which exists in the flow tube. The velocity component due to diffusion (v_d) is given by

$$v_d = Dk_{obs}/v_{lin} \qquad (E2)$$

where D is the diffusion coefficient of methyl radicals and k_{obs} is the overall pseudo-first-order rate constant for the exponential decay of the methyl radicals.[31a] The diffusion coefficient, D, was calculated to be 530 $cm^2\ s^{-1}$ at $T = 298$ K using the Chapman−Enskog formula.[31b] Assuming a $T^{3/2}$ dependence of D on T, we estimate $D = 291\ cm^2\ s^{-1}$ at $T = 200$ K. The range of diffusion corrections was 2−18% at $T = 298$ K falling to 2−7% at $T = 200$ K. To obtain diffusion-corrected experimental times, the decay traces were analyzed on the basis of a simple exponential decay to give a value of k_{obs} which was used to calculate v_d and hence the total flow velocity and reaction time.

Wall Reactions. There are two essentially first-order processes controlling the removal of methyl radicals: reaction with excess D atoms and loss/reaction at the walls. Plots of k_{obs} against [D] indicated that substantially higher wall loss rates were observed for reactions with D atoms than with either simple methyl radical recombination or methyl radical recombination in the presence of H atoms and H_2. It was not possible, therefore, to include a predetermined value for k_{wall} in the analysis program. The two parallel first-order loss processes are very closely correlated, and it proved impossible to separate them in the analysis of a single decay trace. Methyl decays were therefore fitted with a single first-order reaction, that of methyl radicals with D atoms with rate coefficient (k_{tot}). A typical fit is shown as the solid line in Figure 2. The product of k_{tot} and $[D]_{av}$ (the average D atom concentration which varies by less than 10% over the course of a decay) is a pseudo-first-order rate coefficient (k') comprising of two terms

$$k_{tot}[D]_{av} = k_1[D]_{av} + k_{wall} \qquad (E3)$$

A plot of $k_{tot}[D]_{av}$ vs $[D]_{av}$ has k_1 as the gradient and k_{wall} as the intercept (Figure 3a−d). Table 2 summarizes the experimental results.

However, it is worth noting that the ($T = 300$ K) wall loss rates (the intercepts of the bimolecular plots) are all substantially higher (average = 177 ± 70 s^{-1}) than the observed decays of methyl radicals in the presence of H atoms under conditions where methyl radical recombination is insignificant (typical value = 25 ± 10 s^{-1}) The total methyl decays (Figure 1b) appear to agree well with the simulated loss (solid line in Figure 1b) of CH_3 in the presence of H atoms, implying that when D atoms are present the methyl radicals do not remain at the wall but rather the intercept is a measure of a heterogeneous isotope exchange reaction. The linearity of the plots and the approximately consistent nature of the intercept value for each methyl isotopomer indicate that the analysis technique appears to be able to separate the homogeneous and heterogeneous components of the reaction. The presence of a heterogeneous pathway does add a potential uncertainty to the data; however, the heterogeneous component is never more than 10% of the largest pseudo-first-order removal rate for each of the isotopomers.

The statistical errors for the current analysis of reactions 1a−c are of the order of ± 5−10% (1 σ), additional experimental uncertainties (absolute [D] and [methyl], nonuniform concentration distributions during the first 0.5 ms of reaction) and approximations (diffusion velocity corrections, average concentration of D atoms during the decays, and the effects of wall reactions) could realistically extend the absolute uncertainties in the rate coefficients to ±25%.

TABLE 1: Mechanism for Numerical Fitting

reaction	k at 300 K[a]	k at 200 K[a]	comments
$F + CH_4 \rightarrow HF + CH_3$	7.9×10^{-11}	NA	*J. Phys. Chem. Ref. Data* **1992**, *21*, 1125
$F + D_2 \rightarrow DF + D$	9.5×10^{-12}	3.1×10^{-12}	ref 21
$CH_3 + CH_3 \rightarrow C_2H_6$	3.7×10^{-11}	4.7×10^{-11}	ref 28
$F + CH_3$	1.0×10^{-10}	1.0×10^{-10}	Estimate, Same value used for all methyl isomers. Altering k by factor 2 has little effect (<0.1%) on the fit.
$D + F_2 \rightarrow DF + F$	1.2×10^{-12}	2.2×10^{-13}	ref 29
$F + CH_2D_2 \rightarrow DF + CH_2D$	2.8×10^{-11}	NA	Values calculated from comparison of $F + CH_4$ and $F + CD_4$ (ref 30)
$\rightarrow HF + CHD_2$	4.0×10^{-11}		
$F + CHD_3 \rightarrow DF + CHD_2$	4.1×10^{-11}	1.1×10^{-11}	Values calculated from comparison of $F + CH_4$ and $F + CD_4$ (ref 30)
$\rightarrow HF + CD_3$	2.0×10^{-11}	5.6×10^{-12}	
$CH_3 + D \rightarrow CH_2D + H$	floated	NA	
$CH_2D + D \rightarrow CHD_2 + H$	floated	NA	Returned value from $CH_2D + D$ analyses used in analysis of $CH_3 + D$ experiments
$CHD_2 + D \rightarrow CD_3 + H$	floated	floated	Returned value from $CHD_2 + D$ analyses used in analysis of $CH_2D + D$ and $CH_3 + D$ experiments.

[a] Units = cm^3 molecule^{-1} s^{-1}.

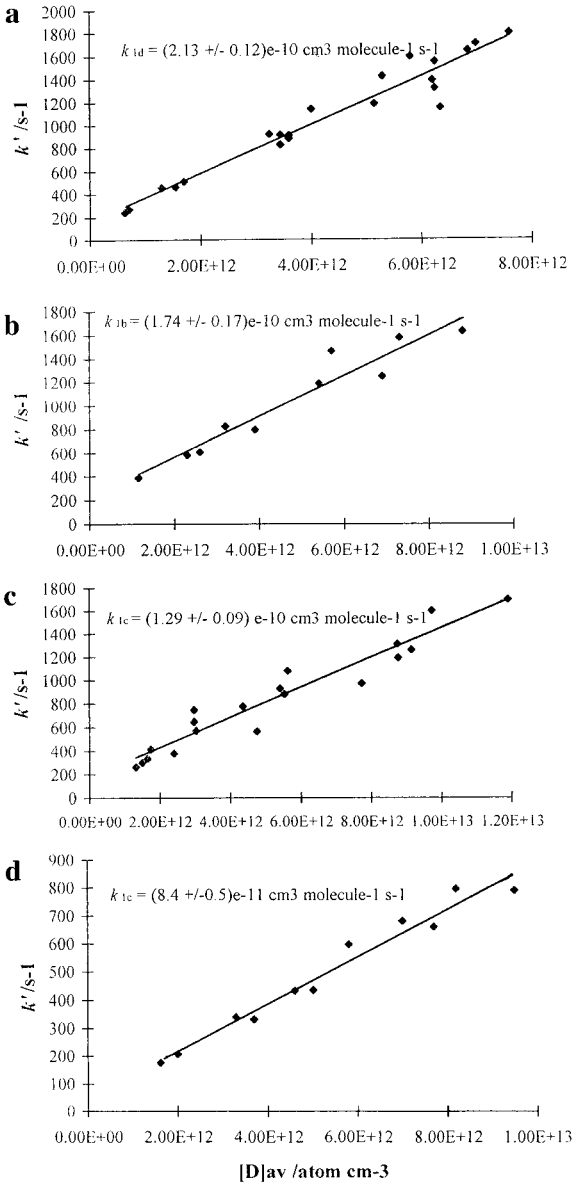

Figure 3. Bimolecular plots for the reactions (a) $CH_3 + D$ at 298 K, (b) $CH_2D + D$ at 298 K, (c) CHD_2 at 298 K, (d) CHD_2 at 200 K. k' is the corrected first-order rate coefficient for methyl removal.

IV. Validity of Isotope Experiments in Determining the High-Pressure Limiting Rate Coefficients

Before continuing with the analysis of the data and a comparison with previous experimental and theoretical determinations, we need to determine what fraction of the high-pressure limit is actually being measured in these experiments, i.e., what is the ratio of the rate coefficients for the decomposition of the methane intermediate forward to products or backward to regenerate reagents? Brouard et al.[15,32] assumed that CH_3D^* always ejected an H atom and justified this assumption for reaction 1a by consideration of the difference in zero-point energies of the two channels ($CH_3 + D$ and $CH_2D + H$). The calculated difference in zero-point energies of $\sim$1200 cm^{-1} leads to an increased sum of states for dissociation to give $CH_2D + H$, which when multiplied by a reaction degeneracy term of 3 for the elimination of an H atoms, means that CH_2D formation is favored substantially over regeneration of reagents. Brouard's calculations were based on estimated values of the vibrational frequencies of CH_2D determined by the product rule and solution of the secular determinant obtained from the approximate force constants for CH_3 and CD_3.[32]

TABLE 2: Summary of Experimental Results[a]

radical	temp/K	range of $[D]_{av} \times 10^{-12}$/atoms cm^{-3}	no. of decays	$k \times 10^{10}$/cm^3 molecule^{-1} s^{-1}	k_{wall}/s^{-1}
CH_3	298	0.63−7.60	21	2.13 ± 0.12	153 ± 58
CH_3[a]	300−400			1.75 ± 0.15[a]	
CH_2D	298	1.15−8.80	10	1.74 ± 0.17	211 ± 92
CHD_2	298	1.32−11.9	19	1.29 ± 0.09	166 ± 53
CHD_2	200	1.61−9.50	11	0.84 ± 0.04	46 ± 30

[a] Errors are statistical at the 1 σ level. [b] Reference 15.

The frequency calculations of Brouard cast significant doubt on the validity of the other isotope experiments as a measure of k_1^∞, as the total zero-point energy difference between CH_3 and CD_3 is only 1670 cm^{-1}. If Brouard's calculations are correct, then there is only $\sim$450 cm^{-1} difference in zero-point energy between CH_2D and CD_3. When combined with the unfavorable reaction degeneracy factor for reaction 1c, one estimates that reaction 1c should be at about 50% of the high-pressure limit.

The use of simple energetic arguments to determine the ratio of forward and reverse rate coefficients (k_H/k_D), and hence to justify the determination of k^∞ from isotope scrambling, is clearly insufficient if the ratio is not substantially greater than unity at accessible energies. The rate coefficients for methane dissociation must be calculated, and this in turn requires determination of the densities of states of the products, reactants, and methane intermediate and a determination of the microcanonical rate coefficients for each channel. Both the density of states and the microcanonical rate coefficient calculations require a knowledge of the vibrational frequencies. In addition,

TABLE 3: Experimental and Calculated Vibrational Frequencies for Methyl Isotopomers

vibration	CH_3 expt/cm^{-1}	CH_3 calc/cm^{-1}	ratio	CD_3 expt/cm^{-1}	CD_3 calc/cm^{-1}	ratio	CH_2D UHF calc/cm^{-1}	CH_2D UHF calc/R cm^{-1}	CHD_2 UHF calc/cm^{-1}	CHD_2 UHF calc/R cm^{-1}
A_2''	606	486	0.80	458	376	0.82	452	558	416	513
E′	1396	1541	1.10	1026	1134	1.11	1290	1167	1140	1032
E′	1396	1541	1.10	1026	1134	1.11	1534	1390	1414	1278
A_1'	3044	3265	1.07	2155	2310	1.07	2474	2312	2388	2232
E′	3162	3453	1.09	2381	2573	1.08	3340	3078	2573	2371
E′	3162	3453	1.09	2381	2573	1.08	3453	3183	3401	3134
zero-point energy	6383			4713				5844		5280

the behavior of the isotopically labeled system must be examined at the experimental pressures using the master equation.

In the absence of experimental determinations of the vibrational frequencies of CH_2D and CHD_2 we have calculated frequencies for the methyl isotopomers using the GAUSSIAN94 ab initio package at the UHF level with a 6-31G basis set.[33] At this low level of calculation the absolute values of the calculated frequencies are not expected to be particularly accurate; however, the relative ratios of vibrational frequencies should be correct, and absolute values can be obtained from ratios of the calculated frequencies for CH_3 and CD_3 with experimental observations.[34−37]

The results of the calculations are presented in Table 3. With the exception of the strongly anharmonic A''_2 "umbrella" motion, the agreement with experiment for both CH_3 and CD_3 is within 10% and is consistent for both CH_3 and CD_3. An average correction factor, *R*, for each set of vibrations was then used to calculate the absolute frequencies of the CH_2D and CHD_2 molecules. As might be expected, the zero-point energies of the methyl isotopomers show a gradual decrease with an average difference of ∼550 cm^{-1} between each isotopomer. The calculated frequencies were used subsequently in the calculation of transition-state partition functions and densities of states.

An estimate of the limits on k_H/k_D can be obtained by examining what happens to the multichannel master equation (ME) in the high- and low-pressure limits (for more details on the master equation see Appendix I). To do this, the time evolution of the population of methane intermediates in different energy "grains" is calculated. In the high-pressure limit, stabilization is complete and the ratio k_H/k_D becomes the ratio of the high-pressure rate coefficients for each channel. In the low-pressure limit (which closely corresponds to the present experimental conditions[15]), the collisional activation/deactivation processes are negligible and the multichannel ME (eq A1) can be simplified to[38]

$$\frac{\partial \rho(E,t)}{\partial t} = -k_H(E)\,\rho(E,t) - k_D(E)\,\rho(E,t) + R(E,t) \quad \text{(E4)}$$

where $k_H(E)$ and $k_D(E)$ are the microcanonical rate coefficients for the dissociation through the channels giving H atoms and D atoms as products, respectively, $\rho(E,t)$ is the probability that a methane molecule will have an energy *E*, and $R(E,t)$ is the source term, i.e., the contribution to the probability density due to the methyl combination reaction with D atoms. The source term is related to the association rate, and as the reagents are in a Boltzmann distribution (more collisions with bath gas than each other), the source term is given by

$$R(E,t) = k_a^{\infty}\,[CH_3][D]\,g(E) \quad \text{(E5)}$$

where k_a^{∞} is the limiting high-pressure rate coefficient for the association reaction and $g(E)$ is given by

$$g(E) = \frac{k_D(E)\,N(E)\exp(-\beta E)}{\int_0^{\infty} k_D(E)\,N(E)\exp(-\beta E)\,dE} \quad \text{(E6)}$$

N(E) being the density of states of the adduct and $\beta = 1/k_B T$.

In the steady-state regime, the rate of change of probability density is zero, and hence the steady-state probability density is

$$\rho_s(E,t) = \frac{R(E,t)}{k_H(E) + k_D(E)} \quad \text{(E7)}$$

Detailed microcanonical rate constants have been calculated for $CH_3 + H$ and $CH_3 + D$ by Aubanel and Wardlaw,[39] but not the other isotopomers. Such calculations are complex and very time-consuming, but the present analysis can be performed via simpler canonical calculations.

The canonical rate coefficient is given by the product of the microcanonical rate coefficient at energy *E* and the probability density at that energy, integrated over all available energies; therefore

$$\frac{k_D}{k_H} = \frac{\int_0^{\infty} k_D(E)\,\rho_s(E,t)\,dE}{\int_0^{\infty} k_H(E)\,\rho_s(E,t)\,dE} \quad \text{(E8)}$$

Combining eqs E5, E6, and E8 gives

$$\frac{k_D}{k_H} = \frac{\int_0^{\infty} k_D(E)\,r(E)\,dE}{\int_0^{\infty} k_H(E)\,r(E)\,dE} \quad \text{(E9)}$$

where $r(E)$ is given by

$$r(E) = \frac{k_D(E)\,N(E)\exp(-\beta E)}{k_H(E) + k_D(E)} \quad \text{(E10)}$$

However, before these equations can be used to calculate the ratio of forward and reverse rate coefficients, the microcanonical rate coefficients $k_H(E)$ and $k_D(E)$ must be supplied. The microcanonical rate coefficients are given by the standard RRKM prescription,

$$k(E) = \frac{W^{\ddagger}(E)}{hN(E)} \quad \text{(E11)}$$

where $W^{\ddagger}(E)$ is the rovibrational sum of states at the transition state and *N(E)* is the rovibrational density of states of the adduct.

$W^{\ddagger}$ is related to the rovibrational partition function of the transition state via a Laplace transform[38]

$$L\,[W^{\ddagger}(E)] = Q_{TS}^{\ddagger}/\beta \quad \text{(E12)}$$

and hence the microcanonical rate coefficients can be calculated

TABLE 4: Corrected Experimental Values of k_{1a-c}

reaction	temp/K	% of H atom ejection at zero pressure	% of high-pressure limit	10^{10} × corrected experimental determination/cm^3 molecule^{-1} s^{-1}
$CH_3 + D$	300	92	92	2.3 ± 0.6[b]
$CH_3 + D$[a]	300	92	94[a]	1.86 ± 0.16
$CH_2D + D$	300		82	2.1 ± 0.5[b]
$CHD_2 + D$	300	67	68	1.9 ± 0.5[b]
$CHD_2 + D$	200	75	76	1.1 ± 0.3[b]

[a] Brouard et al.[32] Ratio of rate coefficients calculated at 100 Torr. [b] Errors are ±25% which is made up of a statistical (±1 σ) component plus 15% for additional uncertainties in the experimental measurements and corrections to the high-pressure limits.

if the partition function of the transition state can be evaluated. The partition function $Q^{\ddagger}_{TS}$ can be written as the product of two partition functions, $Q^{\ddagger}_{c}\ Q^{\ddagger}_{t}$ where the partition function $Q^{\ddagger}_{c}$ represents the conserved modes, i.e., those modes which do not change significantly in character on going from reactants to products, usually vibrations of the separated fragments. The partition function $Q^{\ddagger}_{t}$ is for the transitional modes, i.e., those modes that do change substantially during the course of the reaction; typically they are the free rotations of the separated fragments, which become first hindered rotations and then finally vibrations of the adduct, as well as the overall rotation of the system. The calculation of $Q^{\ddagger}_{c}$ is usually straightforward and is often based on the approximation of separable quantum harmonic oscillators. The calculation of $Q^{\ddagger}_{t}$ is difficult, involving large amplitude motions that couple strongly with overall rotation and which must transform smoothly between free rotation and vibrational limits. Appendix II details the calculation of $W^{\ddagger}(E)$ based on canonical flexible transition-state theory, where $W^{\ddagger}(E)$ is minimized for each energy.

The results of the calculations are given in Table 4. The values in the third column give the percentage of H atom formation at zero pressure (i.e., no stabilization of the methane intermediate), and this represents the "worst case scenario". In the fourth column are the calculated values for the experimental conditions obtained using a full master equation calculation, and it can be seen that, for the present experiments, the results are close to the low-pressure limit. Both calculations come close to justifying the original assumptions made by Brouard et al. for reaction 1a. For the $CH_3 + D$ system at 300 K and 1 Torr, the ratio of forward to reverse reactions is 12:1 and hence the observed reaction is at 92% of the high-pressure limit. At 600 Torr, the highest pressure of the earlier Brouard study, reaction 1a is calculated to be at ~95% of the high-pressure limit.

As would be expected, given the regular changes in zero-point energy of the methyl radicals, the ratios of sums of states for the two dissociation channels remain approximately constant for all of the reactions studied. However, the reaction path degeneracy becomes increasingly unfavorable for the forward reaction (ejection of an H atom) as the deuteration of the methyl radical is increased. The ratio of the sums of states for forward and reverse dissociation for the reactions 1a−c (including reaction path degeneracy) is shown as the solid lines in Figure 4. The ratio decreases rapidly as the energy with which the methane intermediate is formed is increased. The dashed curves show the distribution of methane energies at 300 and 600 K. Close to the reaction threshold the forward reaction is strongly favored for all the reactions 1a−c; however, closer to the mean methane formation energy the ratio of dissociation rates becomes much smaller. Master equation calculations show that, for the reaction of $CHD_2 + D$, the observed reaction is only at 68% of the high-pressure limit at 1 Torr. The appropriate corrections to the experimental rate coefficients are made in the final column of Table 4.

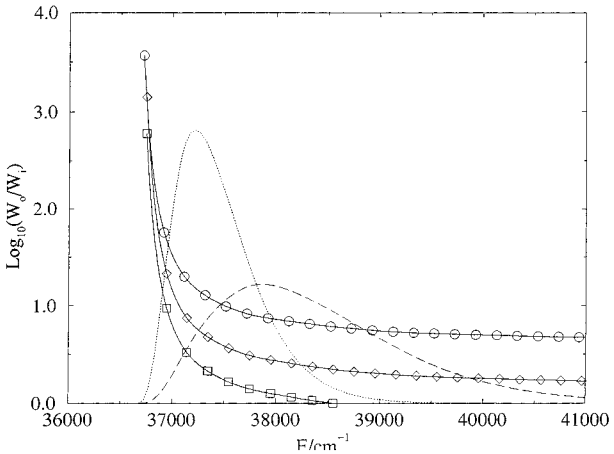

Figure 4. Ratio of sums of states for forward and reverse dissociation (including reaction path degeneracy) of the methane intermediate (solid lines) for reactions 1a−c (○, CH_3D; ◇, CH_2D_2; □, CHD_3) as a function of methane energy. The dashed curves show the energy distribution of the methane intermediates formed by the reactions of methyl + D at 300 K (- - -) and 600 K (— —). The distributions are approximately the same for each methyl isotopomer.

The ratio of forward to reverse methane dissociation is temperature dependent as the temperature, and hence energy, of the reagent species controls the ratio of accessible states for the forward and reverse reactions. As the temperature is lowered, the relative number of accessible reverse states decreases, and hence at 200 K under the experimental conditions, reaction 1c is at 75% of the high-pressure limit.

V. Isotopic Relationships of the Rate Coefficients

The relationship between the high-pressure limiting rate coefficients for the isotopic variants of reaction 1 is best examined via canonical flexible transition-state theory.[4,38] The association rate coefficient is given by

$$k_r^{\infty} = g_e \frac{k_B T}{h} \frac{\sigma}{\sigma^{\ddagger}} \frac{Q'(r,T)}{Q_R(T)} \exp(-\Delta V_{rc}(r)/k_B T) \qquad \text{(E13)}$$

where g_e is the ratio of the electronic degeneracies, $\sigma/\sigma^{\ddagger}$ is the ratio of symmetry numbers for the fragments (methyl and atom) and the transition state, $Q_R(T)$ is the total partition function for the reactants (excluding symmetry numbers), $Q'(r,T)$ that for the transition state with the mode corresponding to the reaction coordinate factored out, and ΔV_{rc} is the potential along the reaction coordinate. Both $Q'(r,T)$ and ΔV_{rc} depend on r, and hence the position of the transition state, $r^{\ddagger}$, is found variationally.

The total partition function for the transition state can be expressed as

$$Q'(r) = Q_{CH_4\ trans} Q'_c(r)\ Q'_t(r) \qquad \text{(E14)}$$

where $Q_{CH_4\ trans}$ is the translational partition function, $Q'_c(r)$ is the partition function of the conserved modes of vibration, i.e., the vibrational frequencies which remain approximately constant in moving from fragments to transition state, and $Q'_t(r)$ is the partition function of the transitional modes plus the external rotations. Robertson, Wagner, and Wardlaw[4] have rigorously shown that the transitional partition function for the transition state can be expanded in terms of a pseudo-diatomic (methyl and hydrogen atom) partition function (Q_{pd}), free rotor partition

TABLE 5: Symmetry and Reduced Masses Used in Calculation of Ratios of Rate Coefficients

reaction	σ	$\sigma^{\ddagger}$	μ
$CH_3 + H$	6	3	$\frac{15 \times 1}{15 + 1}$
$CH_3 + D$	6	3	$\frac{15 \times 2}{15 + 2}$
$CH_2D + D$	2	1	$\frac{16 \times 2}{16 + 2}$
$CHD_2 + D$	2	1	$\frac{17 \times 2}{17 + 2}$

functions of the fragments (obviously only the methyl term, $Q'_{\mathrm{fr\ CH_3}}$, needs to be considered in this case), and a hindering function

$$Q'_{\mathrm{t}}(r) = Q_{\mathrm{pd}}(r)\, Q'_{\mathrm{fr\ CH_3}}(r)\, \Theta(r,T) \qquad \text{(E15)}$$

where $Q_{\mathrm{pd}}(r) = 8\pi^2\mu r^2 k_{\mathrm{B}}T/h^2$ (μ is the reduced mass of the pseudo-diatomic i.e., $m_{\mathrm{CH_3}}m_{\mathrm{H}}/(m_{\mathrm{CH_3}} + m_{\mathrm{H}})$). This is a considerable simplification in the analysis as there is now no need to consider the transitional vibrational modes which are difficult to calculate, due to their strong dependence on r.

Minimizing k_{r}^{∞} gives the location of the transition state and an expression for the high-pressure limiting rate coefficient

$$k_{\mathrm{r}}^{\infty} = g_{\mathrm{c}} \frac{k_{\mathrm{B}}T}{h} \frac{\sigma}{\sigma^{\ddagger}} \frac{\exp(-\Delta V_{\mathrm{rc}}(r^{\ddagger})/k_{\mathrm{B}}T}{Q_{\mathrm{trans}}} \left\{\frac{Q_{\mathrm{c}}^{\ddagger}}{Q_{\mathrm{vibCH_3}}}\right\} \left\{\frac{Q_{\mathrm{pd}}^{\ddagger}\, Q_{\mathrm{frCH_3}}^{\ddagger}}{Q_{\mathrm{frCH_3}}(\infty)}\right\} \Theta \qquad \text{(E16)}$$

where Q_{trans} in eq E16 is $(Q_{\mathrm{trans\ CH_4}}/Q_{\mathrm{trans\ CH_3}}Q_{\mathrm{trans\ H}})^{-1} = (2\pi\mu k_{\mathrm{B}}T)^{3/2}/h^3$.

For the conserved vibrational modes, the vibrational partition functions will be approximately equal, except for the umbrella mode whose frequency changes significantly. In any case, for the temperatures and vibrational frequencies being considered the partition functions of these conserved modes will be close to unity. In addition, if we assume that the geometries of the fragments at infinite separation and at the transition state are identical (a reasonable assumption considering the large values of $r^{\ddagger}$) then free rotational partition functions in the transition state and isolated fragments become equal. For free rotation at large $r^{\ddagger}$, $\Theta = 1$. Equation E16 reduces to

$$k_{\mathrm{r}}^{\infty} = g_{\mathrm{c}} \frac{\sigma}{\sigma^{\ddagger}} \pi(r^{\ddagger})^2 \left(\frac{8k_{\mathrm{B}}T}{\pi\mu}\right)^{1/2} \exp(-\Delta V_{\mathrm{rc}}(r^{\ddagger})/k_{\mathrm{B}}T) \qquad \text{(E17)}$$

A number of assumptions have been made in the derivation. However, we are only interested in ratios of rate coefficients, and some of the errors involved with the assumptions will cancel. As a further verification, ratios of the rate coefficients were also calculated using both canonical and microcanonical methods. For ratios of rate coefficients for the isotopic variants of reaction 1, assuming that the differential effects of ΔV_{rc} are small, the ratio of symmetry numbers and reduced masses are the only pertinent values and are shown in Table 5. It can be seen that the ratio of the symmetry numbers in the fragments and transition state (2:1) is the same for all reactions and hence only the mass effects need to be considered in calculating the ratios of rate coefficients. The results are presented in Table 6 along with canonical and microcanonical calculations.

The results of the isotopic corrections can be used to give three independent estimates of the high-pressure limiting rate coefficient. The calculations are summarized in Table 7. The

TABLE 6: Ratios of Rate Coefficients at 300 K

reactions	calculated via ratios of reduced masses	calculated via canonical rate theory	calculated via microcanonical rate theory
$\frac{k^{\infty}_{\mathrm{CH_3+H}}}{k^{\infty}_{\mathrm{CH_3+D}}}$	1.37	1.39[41]	1.38[39]
$\frac{k^{\infty}_{\mathrm{CH_3+H}}}{k^{\infty}_{\mathrm{CH_2D+D}}}$	1.38		
$\frac{k^{\infty}_{\mathrm{CH_3+H}}}{k^{\infty}_{\mathrm{CH_2+D}}}$	1.38		1.39

TABLE 7: Experimental and Calculated Isotopic Ratios for Reactions 1a−c

reaction	calculated $k_{\mathrm{CH_3+D}}/k_{\mathrm{reaction}}$	experimental $k_{\mathrm{CH_3+D}}/k_{\mathrm{reaction}}$	$10^{10} \times k_1^{\infty}$/ molecule^{-1} cm^3 s^{-1}
$CH_3 + D$			3.2 ± 0.8[a]
$CH_3 + D$[b]			2.55 ± 0.21[a,b]
$CH_2D + D$	1.00	1.1 ± 0.5	2.9 ± 0.7[c]
$CHD_2 + D$	1.00	1.2 ± 0.7	2.6 ± 0.7[c]
$CHD_2 + D$[d]	1.00		1.5 ± 0.4[c,d]

[a] Value obtained by mulitplying k_{1a} by appropriate correction factors for D atom (1.37) substitution. [b] From experimental value of Brouard et al.[15] [c] Value obtained by multiplying k_{1b} by appropriate correction factors for D atom and CH_2D substitution (1.38). [d] 200 K values.

second and third columns compare the calculated and experimental ratios of the reactions of the various methyl isotopomers with deuterium. The results of the experimental determinations are in agreement with the calculations; however, being a ratio, the experimental ratio is subject to a significant error. An independent estimate of k_1^{∞} is obtained by multiplying k_{1a-c}^{∞} by the appropriate value for deuterium/hydrogen atom substitution, and the results are presented in the fourth column of Table 7. Combining these gives an average value of k_1^{∞} of $(2.9 \pm 0.7) \times 10^{-10}$ molecule^{-1} cm^3 s^{-1} where the errors (~25%) are estimates of both the statistical and systematic errors in the measurements and calculations.

VI. Master Equation Modeling of the CH_3 + H Data of Brouard et al.

The advances in theories of association reactions,[38] processor power and software techniques makes a reanalysis of the data reported by Brouard et al.[15] a worthwhile exercise. The approach we adopt here is based on the master equation, which has been extensively discussed elsewhere.[38] A brief description and further references may be found in Appendix I.

Before any determination of the overall rate coefficients at various temperatures and pressures can be prosecuted, the microcanonical rate coefficient *k(E)* has to be specified. Two sets of values were used in the calculations, one obtained from the flexible transition-state theory (FTST) and the other from the inverse Laplace transform (ILT), each of which are now discussed in turn. It is assumed in both calculations that all degrees of freedom, including the external rotations, are active. It can be argued that some degrees of freedom should be treated adiabatically; however, for this to occur, the minimum requirement would be a well-defined transition state, which is not the case for reactions such as CH_3 + H.

VI.a. FTST. In their study of CH_3/H recombination Aubanel and Wardlaw[39] used the FTST technique to calculate

TABLE 8: Summary of Fitting to CH_3 + H Data of Brouard et al.[15]

method	k_1^∞	parameters	χ^2
master equation, $k(E)$ from ref 39, $\langle\Delta E_d\rangle = 210(T/300)^m$ cm^{-1}	calculated from results of ref 39, can be parametrized as $k_1^\infty = 2.55 \times 10^{-10}(T/300)^{0.21}$ cm^3 molecule^{-1} s^{-1}	$m = 0.6$	49.7
ILT, $\langle\Delta E_d\rangle = 210(T/300)^m$ cm^{-1}	$k_1^\infty = A(T/300)^n$ cm^3 molecule^{-1} s^{-1}	$A = 3.0 \times 10^{-10}$ cm^3 molecule^{-1} s^{-1} $n = 0.9$ $m = 0.5$	38.6
k_1^∞ 300 fixed by expt, temperature dependence of k_1^∞ and $\langle\Delta E_d\rangle$ floated	$k_1^\infty = 2.9 \times 10^{-10}(T/300)^n$ cm^3 molecule^{-1} s^{-1}	$n = 0.8$ $m = 0.5$	40.3

the transition-state sum of states, $W^{\ddagger}(E,J)$, using the ab initio surface calculated by Hirst[40] and fitted by Hase et al.[41] Analysis of two-dimensional master equations, describing collisional relaxation of E and J, is complex and is not justified in the present context. Microcanonical rate coefficients dependent on energy are therefore required, and so a spline fit to the $W^{\ddagger}(E,J)$ function followed by numerical integration over the J dependence $(2J+1)$ was used to obtain $W^{\ddagger}(E)$ from which $k(E)$ follows from the standard RRKM expression,

$$k(E) = \frac{W^{\ddagger}(E)}{hN(E)} \tag{E11}$$

These rate coefficients were used with no further adjustment to fit the data of Brouard et al.[15] The criterion for the best fit is the minimum in χ^2 formed from the experimental and calculated values. From previous studies it has been shown that the parameter $\langle\Delta E\rangle_d$ is a temperature-dependent function.[42,43] It was represented as

$$\langle\Delta E\rangle_d = 210(T/300)^m \tag{E18}$$

a value of $\sim$200 cm^{-1} is typical of room temperature values of $\langle\Delta E\rangle_d$, although a range of values have been obtained.[43] Indeed, some initial fits were performed with a variety of temperature-independent values of $\langle\Delta E\rangle_d$; however, it rapidly became apparent that temperature variation was the key component in obtaining a good fit. The parameter m was the only parameter that was floated, and a best fit value of 0.6 was obtained. The results of all the fits are summarized in Table 8, and Figure 5a shows a plot of the experimental data of Brouard et al. together with fall off curves obtained from the best fit. As can be seen, the fit is acceptable.

VI.b. ILT. The ILT technique has been extensively studied and tested and has been found to be a robust method, when combined with the ME, of extracting parameters from experimental data.[44] The basis of the approach is the observation that the canonical high-pressure dissociation rate coefficient can be written in terms of a Laplace transform:

$$k_d^\infty(\beta) = \frac{1}{Q(\beta)}\int_0^\infty k(E)\, N(E)\, \exp(-\beta E)$$

$$k_d^\infty(\beta) = \frac{1}{Q(\beta)}\, L\,[k(E)\, N(E)] \tag{E19}$$

As has been described elsewhere,[45] it is often more convenient to apply ILT using the corresponding association high-pressure rate coefficient, thus if the association rate coefficient is of the form

$$k_a^\infty(\beta) = A^\infty \beta^{-n^\infty} \exp(-\beta E^\infty) \tag{E20}$$

The microcanonical rate coefficient for dissociation is given by

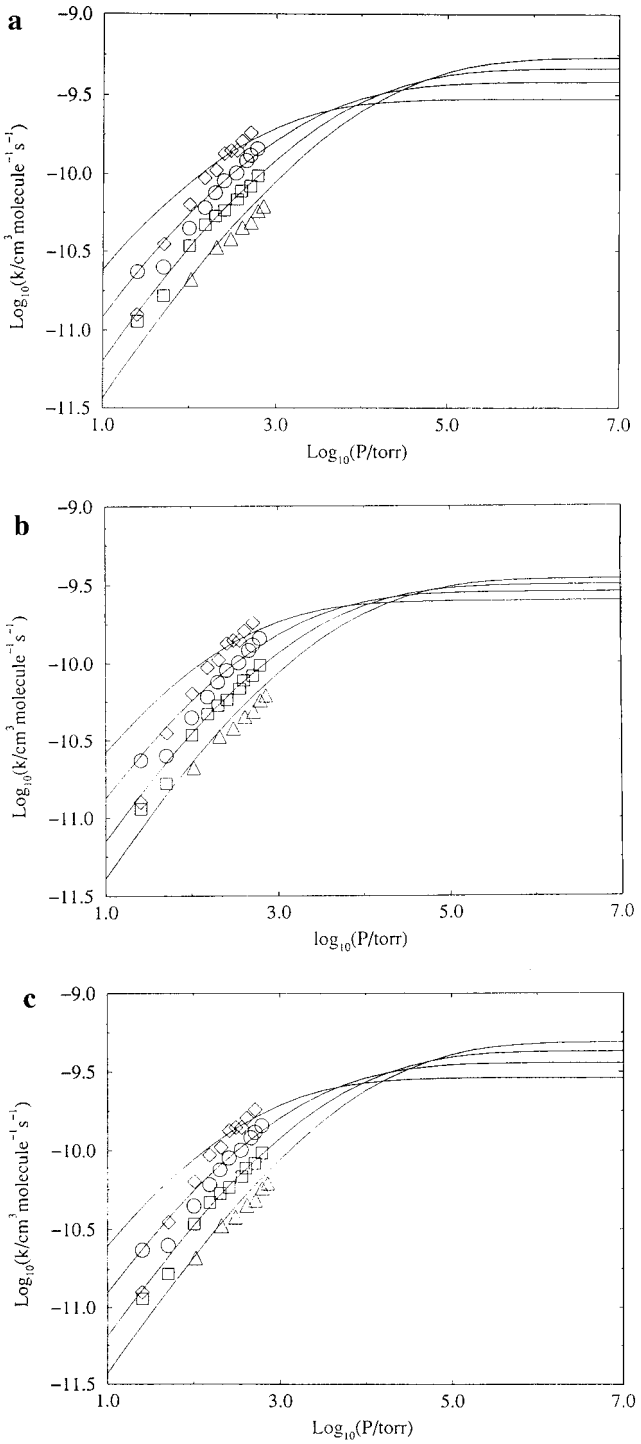

Figure 5. Master equation fits to the CH_3 + H data of Brouard et al.[12] Microcanonical rate coefficients calculated from (a) FTST, (b) inverse Laplace transform, and (c) k_1^∞ at 300 K fixed to experimental value (2.9×10^{-10} cm^3 molecule^{-1} s^{-1}), temperature dependence of k_1^∞ floated. Experimental data points ◇, 300 K; ○, 400 K; □, 500 K; △, 600 K.

$$k(E) = \frac{A^{\infty}C}{N(E)\Gamma(n^{\infty} + 1.5)} \times$$

$$\int_0^{E-E^{\infty}-\Delta H_0^0} N_p(x)[(E - E^{\infty} - \Delta H_0^0) - x]^{n^{\infty}+0.5}\,dx \quad \text{(E21)}$$

where $N_p(x)$ is the convoluted density of states of the two separated fragments and ΔH_0^0 is the zero-point energy difference of the reactants and products. C is given by

$$C = \left(\frac{2\pi M_H M_{CH_3}}{h^2(M_H + M_{CH_3})}\right)^{3/2} \quad \text{(E22)}$$

where M_H and M_{CH_3} are the masses of the two fragments.

The ILT was applied to the data of Brouard et al. The parameter E^{∞} was assumed to be zero as there is no potential barrier to recombination. The parameters that where floated were A^{∞}, n^{∞}, and again the parameter m used to govern the temperature dependence of $\langle\Delta E\rangle_d$ in eq 21. The resulting parameters are presented in Table 8, and the best fit to the data is shown in Figure 5b. It can be seen that the fit is comparable in quality to that obtained using FTST.

VI.c. k_1^{∞} (300 K) Constrained by Experiment. The final fit, shown in Figure 5c, was obtained by constraining the value of A^{∞} to the experimental value obtained in this study (2.9×10^{-10} cm^3 molecule^{-1} s^{-1}) and floating the temperature dependence of the energy transfer parameter and k_1^{∞}. The resulting fit is comparable in quality (as measured by χ^2) with the unconstrained ILT fit.

In summary, all the three fitting methods produce fits to the CH_3 + H data of comparable quality. Not surprisingly, considering the number of floated parameters, the value of χ^2 is somewhat lower for the three-parameter ILT fit and the highest value of χ^2 is obtained when k_1^{∞} is completely constrained in the initial master equation calculations. More importantly, however, are the temperature and pressure dependence of the fall off curves: in the fall off region, these curves reflect the negative temperature dependence of the observed rate coefficients, yet at the limit of high pressures they have a positive temperature dependence, although for the FTST fitting, this merely reflects the calculations of Aubanel and Wardlaw. The calculated values of k_1^{∞} can be parametrized in an $A(T/300)^n$ format (Table 8); however the quality of this fit is not good. The temperature dependence of reaction 1 appears more complex than this simplistic formula, and this needs to be further investigated in order to provide the parametrized form of k_1^{∞} which is required by modelers.

In the original analysis by Brouard et al.,[15] the data were fitted *at each temperature* using a master equation technique, coupled with a variational RRKM analysis of $k(E)$. The data at 300 K led to a high value of k_1^{∞} because of the rapid decrease in k_1 at low pressures. This analysis in turn led to the apparent isotope anomaly when k_1^{∞} was compared with k_{1a}^{∞}. The present analysis uses a *global* fit, over all temperatures, so that the low-pressure data at 300 K have a smaller fractional weight in the overall fit, compared with their weight in the fit by Brouard et al. at 300 K. The global fit is clearly compatible with a positive temperature dependence in k_1^{∞} and with the isotope studies. However, it shows a poor fit to the Brouard k_1 data at 300 K and at low pressures. The origin of this disagreement is not clear and may be related to a systematic error in the experiment under these conditions. Further experiments on CH_3 + H at low pressures would be of value.

VII. Discussion

The present experimental value for k_{1a} at $T = 300$ K, $(2.3 \pm 0.6) \times 10^{-10}$ cm^3 molecule^{-1} s^{-1}, is in agreement with the determination of Brouard et al.[15] who reported temperature- and pressure-independent values for k_{1a}^{∞} of $(1.75 \pm 0.15) \times 10^{-10}$ cm^3 molecule^{-1} s^{-1} over the range 50−600 Torr and 300−400 K, the errors including both a statistical analysis and an estimate of systematic errors in the experiment and analysis. The present master equation analysis on the forward and reverse rate coefficients for CH_3D dissociation indicates that a small correction factor (1.06) should be applied to the Brouard value to account for the minor contribution of the redissociation of the CH_3D intermediate to reagents giving a revised value of $(1.86 \pm 0.16) \times 10^{-10}$ cm^3 molecule^{-1} s^{-1}. Therefore within the experimental limits of the two determinations, there is good agreement for k_{1a}^{∞}.

There are no other direct measurements of reaction 1a and the present results are the first determinations for reactions 1b and 1c. A more detailed review of previous studies of reaction 1, briefly described in section I, can be found in refs 15 and 32. These previous determinations are indirect and in many cases (especially those based on the dissociation of methane), far from the high-pressure limit.

It is noticeable that there is a slight downward trend in the estimates of k_1^{∞} from reactions 1a−c (Table 7, column 4). The magnitude of the random errors is such that it precludes us from determining whether this trend is the result of systematic errors in either the experimental measurements (which are comparatively lower for reactions 1b and 1c) or the calculations of the ratios of dissociation rates for the methane intermediates or simply the uncertainties in the experiment and calculations. We use a simple average of three isotopic determinations of k_1^{∞} to give an overall estimate, as reactions 1b and 1c have slightly lower experimental errors compared to 1a but are significantly further from the high-pressure limit and so are subject to greater uncertainty in converting the experimentally determined values of $k_{1b,c}$ to $k_{1b,c}^{\infty}$.

Theoretical calculations of k_1^{∞} are in good agreement with the two direct studies of reaction 1a (Table 9). Most recently Robertson, Wagner, and Wardlaw[4] have calculated a value of 2.66×10^{-10} cm^3 molecule^{-1} s^{-1} for k_1^{∞} using canonical flexible transition-state theory. The potential energy surface upon which the calculations were performed accounted for the interactions between the incoming atom and the hydrogen atoms of the methyl radical. The potential is at its lowest when the attacking H atom passes between two C − H bonds and

TABLE 9: Comparison between Theoretical and Experimental Determinations

	CH_3 + H						CH_3 + D		
reaction	μFTST[a]	CFTST[b] Robertson[b]	CTST[c] Hirst[c]	CTST[b] Brown/Truhlar[d]	CTST[b] Schlegel[e]	expt	μFTST[a]	CTST[c] Hirst[c]	expt
k^{∞} at 200 K[f]		2.21	2.28	2.49	1.71	1.5 ± 0.4[g]		1.65	
k^{∞} at 300 K[f]	2.36	2.66	2.64	2.74	1.99	2.6 ± 0.7[g]	1.71	1.89	$2.3 \pm 0.6k_1^{\infty}$

[a] Microcanonical flexible transition-state theory. [b] Canonical flexible transition-state theory.[4] [c] Canonical transition-state theory.[41] [d] Reference 47. [e] Reference 48. [f] $10^{10} \times k$/cm^3 molecule^{-1} s^{-1}. [g] From experimental determination of k_{1c} and appropriate isotope correction.

effectively reduces the cone of acceptance for the reaction. This approach is a development of earlier work where the methyl radical was effectively treated as a disk[46] and reduces k_1^∞ by approximately 30%.

As with most theoretical calculations, Robertson et al.[4] predict a positive temperature dependence with the calculated value of k_1^∞ at 200 K being 2.21×10^{-10} cm^3 molecule^{-1} s^{-1}. On the basis of our experimental study of reaction 1c and making the appropriate isotope corrections we calculate a value of $k_1^\infty(200\ \mathrm{K}) = (1.5 \pm 0.4)\ 10^{-10}$ cm^3 molecule^{-1} s^{-1}, in reasonable agreement with the theoretical calculations at the lower temperature. However, the temperature dependence of reaction 1, calculated from studies of reaction 1c, would appear to be greater than that predicted from theoretical calculations. Interestingly the fits to the $CH_3 + H$ data of Brouard, where the temperature dependence of k_1^∞ is unconstrained, also lead to stronger temperature dependencies.

The calculations of Robertson et al.[4] predict a 16% increase in k_1^∞ over the temperature range (300−400 K) studied by Brouard et al.[15] for reaction 1a. This is significantly greater than the reported statistical uncertainty by Brouard et al.; however, studies at the higher end of their temperature range were subject to larger errors and the resulting uncertainty could mask a slight temperature dependence.

Hase et al.[41] also performed canonical transition-state theory calculations using a number of potential energy surfaces. Once again the results appear to be in good agreement with experiment and show the positive temperature dependence expected for this reaction. They also made direct calculations of the values for the $CH_3 + D$ reaction, the ratio k_1^∞/k_{1a}^∞ being 1.39.

VIII. Conclusions

Reactions 1a−c have been directly studied using discharge flow coupled with mass spectrometric monitoring and produce an internally consistent set of results. The absolute value for reaction 1a is in good agreement with the earlier direct determination by Brouard et al.[15] A new value of $k_1^\infty(300\ \mathrm{K}) = (2.9 \pm 0.7) \times 10^{-10}$ cm^3 molecule^{-1} s^{-1} is recommended and the positive temperature dependence of reaction 1 obtained in theoretical studies is confirmed. This analysis is based on new fits to the data of Brouard et al. coupled with the new experimental data reported here. The fits show poor agreement with the low-pressure data for the $CH_3 + H$ reaction at low temperatures, and it is suggested that there may be some systematic experimental error under these conditions. Experiments at higher temperatures than are feasible with the present apparatus are required to determine k_1^∞ under combustion conditions.

Acknowledgment. This work was supported by the NASA Planetary Atmospheres Program. P.W.S. acknowledges support for his visit to NASA/GSFC from the University of Leeds and from NASA/GSFC via the Universities Space Research Association (USRA). R.P.T. thanks the National Academy of Science for the award of a Resident Research Associateship. F.L.N. acknowledges support under NASA cooperative agreement NCC5-68 with the Catholic University of America. We would like to thank Jun Gang for performing the GAUSSIAN calculations.

Appendix I. Master Equation Calculations

The form of the ME equation used to examine the combination of CH_3 and H atoms is

$$\frac{\partial\rho(E,t)}{\partial t} = \omega\int_0^\infty P(E|E')\,\rho(E',t) - \omega\rho(E,t) - k(E)\,\rho(E,t) + R(E,t) \quad \text{(A1)}$$

where $\rho(E,t)$ is the probability that a CH_4 molecule will have an energy E, ω is the collision frequency, $P(E|E')$ is the transition density from energy E' to energy E, $k(E)$ is the microcanonical dissociation rate coefficient, and $R(E,t)$ is the source term, i.e., the contribution to the probability density due to the combination reaction. As in previous studies,[43,44,49] the collision frequency is taken to be the Lennard-Jones collision frequency and the kernel $P(E|E')$ is assumed to have the exponential down form, such that the probability of a deactivating collision is given by

$$P(E|E') = A(E')\exp(-\alpha(E - E')) \qquad E \le E' \quad \text{(A2)}$$

where $\alpha^{-1} = \langle\Delta E\rangle_d$, $\langle\Delta E\rangle_d$ being the average energy transferred in a downward collision. The probability of activating collisions is found by applying detailed balance.

The source term $R(E,t)$ is constructed on the assumption that the reactants are always in a Boltzman distribution and has been shown to be (eqs 5 and 6, section V)

$$R(E,t) = k_a^\infty\,[CH_3][H]\,g(E) \quad \text{(A3)}$$

with the terms k_a^∞ and $g(E)$ being defined above.

The complexity of the state space means that the solution of eq A1 must be performed numerically, and the graining technique described elsewhere[38] was adopted here. Briefly, the energy axis of the system was split into a set of contiguous grains that assigned state numbers, a mean energy, and mean microcanonical rate coefficient. The continuous density ρ is replaced by a vector, $\boldsymbol{\rho}$, the elements of which are the probabilities for a molecule to be found in a given grain. With this approximation the ME equation can be rewritten in matrix form as

$$\mathrm{d}\rho/\mathrm{d}t = \omega[\mathbf{P} - \mathbf{I}]\rho - \mathbf{K}\rho + R'(t)\mathbf{g} \quad \text{(A4)}$$

where $\mathbf{P}$ is the collision matrix describing the probability of movement between grains on collision, $\mathbf{I}$ is the identity matrix, $\mathbf{K}$ is a diagonal matrix of the grain averaged $k(E)$, $\mathbf{g}$ is a vector representation of the function $g(E)$, and the definition of $R'(t)$ follows from eq 6. Equation A4 is nonlinear in t but can be solved in the steady state. The solution for this regime, $\boldsymbol{\rho}_s$ being given by

$$\boldsymbol{\rho}_s = -R'(t)\,\mathbf{M}^{-1}\mathbf{g} \quad \text{(A5)}$$

where $\mathbf{M} = \omega[\mathbf{P} - \mathbf{I}] - \mathbf{K}$. Finally, the overall rate coefficient of association can be found by the introduction of an absorbing boundary at an energy sufficiently far below the threshold that reactivation to states above the threshold is negligible.

Appendix II. Calculations of the Sum of States for the $CH_3 + H$ Transition State

Following the discussion of $Q_c^\ddagger$ and $Q_t^\ddagger$ begun in sections IV and V, the division of modes can be carried over into the calculation of $W^\ddagger(E)$ by use of the convolution theorem:

$$W^\ddagger(E) = \int_0^E W_t^\ddagger(E - x)N_c^\ddagger(x)\,\mathrm{d}x$$

$$W^\ddagger(E) = \int_0^E W_c^\ddagger(E - x)N_t^\ddagger(x)\,\mathrm{d}x$$

$$W^\ddagger(E) = \int_0^E \mathrm{d}y\int_0^y N_t^\ddagger(y - x)N_c^\ddagger(x)\,\mathrm{d}x \quad \text{(A6)}$$

In practical terms eq A6 means that $W^{\ddagger}(E)$ can be obtained by first calculating $N_t^{\ddagger}(E)$, the density of states of the transitional modes, storing it in numerical form, and then executing a direct count algorithm upon this stored numerical form which will have the effect of simultaneously calculating $N_c^{\ddagger}(E)$ and convolving it with $N_t^{\ddagger}(E)$. This approach was adopted here.

In a recent paper Robertson et al.[4] presented a general approach to the calculation of $Q_t^{\ddagger}$ based on earlier work of Aubanel et al.[46] or Wardlaw et al.[50−53] The point of departure for the calculation of $Q_t^{\ddagger}$ is the classical canonical partition function

$$Q_t^{\ddagger} = \frac{1}{h''}\int \exp(-\beta H_t(\mathbf{p},\mathbf{q}))\, d\mathbf{p}\, d\mathbf{q} \qquad (A7)$$

where n is the number of transitional modes, H_t is the classical Hamiltonian for the transitional modes, **q** is the set of generalized coordinates, and **p** is the conjugate momenta. If the kinetic energy term of H_t can be written in a quadratic form, then the theorem of Aston and Eidinoff[54] allows the integration over momenta to be performed analytically. If, in addition, H_t is defined in terms of a new set of body fixed coordinates, then integration over the cyclic Euler coordinates can, in the absence of any external fields, also be performed analytically. The resulting expression after these manipulations is

$$Q_t^{\ddagger} = \frac{8\pi^2}{\sigma}\left(\frac{2\pi}{\beta h^2}\right)^{n/2}\int \sqrt{|\mathbf{A}|}\, \exp(-\beta V_t(\mathbf{q}))\, d\mathbf{q} \qquad (A8)$$

where $|\mathbf{A}|$ is the determinant of the generalized inertial tensor, the terms of which have been discussed in detail by Robertson et al.,[4] V_t is the potential associated with the transitional modes, and **q** now refers to those transitional modes that exclude rotation of the body fixed frame.

Equation A8 is a Laplace transform and can be inverted to give a general expression for the transitional mode density of states. Such an inversion and its connection to the work of Smith[55] has been discussed by Robertson et al.[4] Here, a specific expression for the system under discussion is derived based on the approximate potential used by Aubanel et al.[46]

For the CH_3/H association reaction, $n = 5$ and the integral in eq A8 is of two dimensions. The set of coordinates used by Aubanel et al.[39] are adopted here. In brief, a set of body fixed axes are attached to the system such that the origin is at the center of mass of the overall system with the z-axis lying along the vector that joins the CH_3 center of mass with the H atom. Two angles are needed to describe the orientation of the CH_3 to the body-fixed axes: γ is the angle between the C_3 axis of the methyl group and the body-fixed z-axis and ϕ is the angle of rotation of the C_3 axis. These two angles form the dimensions of the integral, and so V_t is written in terms of them. Following Aubanel et al.,[46] V_t is approximated by

$$V(\gamma) = V_0(R)\sin^2\gamma \qquad (A9)$$

there being no dependence on ϕ. The barrier height to the rotation through γ is V_0 and, as indicated, is a function of the reaction coordinate R, increasing as R decreases. The value of $|\mathbf{A}|$ is given by

$$|\mathbf{A}| = I_a I_b^2(\mu R^2)^2 \sin^2\gamma \qquad (A10)$$

where I_a and I_b are the principal moments of inertia of CH_3, μ is the reduced mass of the associating species, and R is the distance between their centers of mass. Substitution of these expressions into eq A8 followed by integration over ϕ gives

TABLE 10: Sum of States at the Transition State for $CH_3 + H \rightarrow CH_4$

$(E - \Delta H_0^0)$/ cm^{-1}	$W^{\ddagger}(E)$ (FTST)	$W^{\ddagger}(E)$ (this work)	% difference	R/Å
155	704	986	+40	3.85
248	2838	3193	+13	3.75
413	10679	11334	+6	3.65
624	31886	30973	−3	3.60
1040	1.291×10^{05}	1.164×10^{05}	−10	3.55
1248	2.165×10^{05}	1.914×10^{05}	−12	3.50
2007	9.125×10^{05}	8.066×10^{05}	−12	3.45
2080	1.020×10^{06}	9.089×10^{05}	−11	3.40
2600	2.174×10^{06}	1.952×10^{06}	−10	3.35
3120	4.1040×10^{06}	3.759×10^{06}	−8	3.30
3419	5.848×10^{06}	5.306×10^{06}	−9	3.25
4015	1.064×10^{07}	1.006×10^{07}	−5	3.15
4445	1.611×10^{07}	1.535×10^{07}	−5	3.10
5554	4.176×10^{08}	4.093×10^{08}	−2	2.95

$$Q_t^{\ddagger}(\beta R) = \frac{16\pi^3}{\sigma}\left(\frac{2\pi}{\beta h^2}\right)^{5/2}\sqrt{I_a I_b^2}\mu R^2\int_0^{\pi}\sin\gamma \exp(-\beta V_0(R)\sin^2\gamma)\, d\gamma \qquad (A11)$$

If $A(R)$ is defined to be

$$A(R) = \frac{16\pi^3}{\sigma}\left(\frac{2\pi}{\beta h^2}\right)^{5/2}\sqrt{I_a I_b^2}\mu R^2 \qquad (A12)$$

then the density of states of the transitional modes from eq A6 is given by

$$N_t^{\ddagger}(E,R) = \frac{A(R)}{\Gamma(5/2)}\int_0^E (E-x)^{3/2}h(x)\, dx \qquad (A13)$$

where the convolution theorem of Laplace transforms has been employed and $h(x)$ is given by

$$h(x) = \int_0^{\pi}\sin\gamma\,\delta\,(x - V_0(R)\sin^2\gamma)\, d\gamma \qquad (A14)$$

It can be shown that $h(x)$ has the following form,

$$h(x) = (V_0^2 - xV_0)^{-1/2} \qquad x < V_0$$

$$h(x) = 0 \qquad x \geq V_0 \qquad (A15)$$

The convolution in eq A8 can be done analytically. Two separate cases need to be considered, that for when $E < V_0$ and that for when $E \geq V_0$. The formulas for these two cases, obtained using MAPLE, are rather cumbersome. The potential barrier V_0 used in these calculations was the fit given by Aubanel et al.[46] to the ab initio data of Hirst.[40]

Having obtained the density of states for the transitional modes, the conserved modes were added, as described above, by executing a standard Beyer−Swinehart algorithm upon a stored numerical form of $N_t^{\ddagger}(E,R)$. A cell size of 1 cm^{-1} was used for this calculation. The frequencies used in a the Beyer−Swinehart procedure were assumed to be those in methane with the exception of the umbrella mode which changes significantly in going over to products and which was represented as a function of R by an exponential interpolation as proposed by Wardlaw and Marcus.[51] The overall density of states was then integrated numerically to give $W_t^{\ddagger}(E,R)$. The values of $W_t^{\ddagger}(E,R)$ were calculated for each cell at series of grid points along the reaction coordinate R at 0.05 Å intervals, and the minimum values of $W_t^{\ddagger}(E,R)$ determined.

Table 10 shows a comparison of the values calculated from this approach and the values calculated form the full FTST

calculations of Aubanel and Wardlaw, for selected energies. The calculations of Aubanel and Wardlaw accounted for the J dependence of $W_t^{\ddagger}(E,R)$, and the values presented here are obtained by integration over the J dependence to give a function only in E. While the agreement is not exact, it is reasonable, the sources of disagreement being the crudeness of the potential, the lack of J conservation, and the original uncertainties in the Aubanel and Wardlaw results due to the Monte Carlo procedure used to perform the phase integral. Also shown in Table 10 are the values of R for which the minimum in $W_t^{\ddagger}(E,R)$ occurred.

References and Notes

(1) Pilling, M. J.; Robertson, S. H.; Seakins, P. W. *J. Chem. Soc., Faraday Trans*. **1995**, *91*, 4179.

(2) Warnatz, J. In *Combustion Chemistry*; Gardiner, J., Ed.; Springer-Verlag: New York, 1983.

(3) Herbst, E.; Leung, C. M. *Astro. J. Suppl.* **1989**, *69*, 271.

(4) Robertson, S. H.; Wagner, A. F.; Wardlaw, D. M. *J. Chem. Phys.* **1995**, *103*, 2917.

(5) Hughes, K. Private Communication.

(6) Kee, R. J.; Rapley, F. M.; Miller, J. A. CHEMKIN-2 Fortran Chemical Kinetics package for the analysis of gas-phase chemical kinetics. Sandia Report SAND89-8009B, 1991.

(7) Gladsone, G. R.; Allen, M.; Yung, Y. L. *Icarus* **1996**, *119*, 1.

(8) Pratt, G.; Veltmann, I. *J. Chem. Soc., Faraday Trans. 1* **1976**, *72*, 1733.

(9) Brown, J. M.; Coates, P. B.; Thrush, B. A. *Chem. Commun.* **1966**, 843.

(10) Dodonov, A. F.; Lavrovskaya, G. K.; Tal'zrose, V. L. *Kinet. Catal. (USSR)* **1969**, *10*, 391.

(11) Cheng, J. T.; Yeh, C. T. *J. Phys. Chem.* **1977**, *81*, 1982.

(12) Pilling, M. J.; Robertson, J. A.; Rogers, G. R. *Int. J. Chem. Kinet.* **1976**, *8*, 883.

(13) Patrick, R.; Pilling, M. J.; Rogers, G. R. *Chem. Phys.* **1980**, *53*, 279.

(14) Sworski, T. J.; Hochanadel, C. T.; Ogren, P. J. *J. Phys. Chem.* **1980**, *84*, 129.

(15) Brouard, M.; Macpherson, M. T.; Pilling, M. J. *J. Phys. Chem.* **1989**, *93*, 4047.

(16) Brouard, M.; Macpherson, M. T.; Pilling, M. J.; Tulloch, J. M.; Williamson, A. P. *Chem. Phys. Lett.* **1985**, *113*, 413.

(17) Brouard, M.; Pilling, M. J. *Chem. Phys. Lett.* **1986**, *129*, 439.

(18) Macpherson, M. T.; Pilling, M. J.; Smith, M. J. C., *J. Phys. Chem.* **1985**, *89*, 2268.

(19) Brunning, J.; Stief, L. J. *J. Chem. Phys.* **1986,** *84*, 4371.

(20) Nesbitt, F. L.; Payne, W. A.; Stief, L. J. *J. Phys. Chem.* **1988**, *92*, 4030.

(21) Stevens, P. S.; Brune, W. H.; Anderson, J. G. *J. Phys. Chem.* **1989**, *93*, 4068.

(22) Baulch, D. L.; Cobos, C. J.; Cox, R. A.,; Eser, C.; Frank, P.; Just, Th.; Kerr, J. A.; Pilling, M. J.; Troe, J.; Walker, R. W.; Warnatz, J. *J. Phys. Chem. Ref. Data* **1992**, *21*, 1125.

(23) Worsdorfer, U.; Heydtmann, H. *Ber. Bunsen-Ges. Chem.* **1989**, *93*, 1132.

(24) Appelman, E. H.; Clyne, M. A. A.; *J. Chem. Soc., Faraday Trans. 1* **1975**, *71*, 2072.

(25) Marston, G.; Nesbitt, F. L.; Nava, D. F.; Payne, W. A.; Stief, L. J. *J. Phys. Chem.* **1989**, *93*, 5769.

(26) Jaffe, S.; Clyne, M. A. A. *J. Chem. Soc., Faraday Trans. 2* **1981**, *77*, 531.

(27) Pilling, M. J.; Smith, M. J. C. *Chem. Phys. Lett.* **1983**, *94*, 430.

(28) Slagle, I. R.; Gutman, D.; Davies, J. W.; Pilling, M. J. *J. Phys. Chem.* **1988**, *92*, 2455.

(29) Cohen, N.; Westberg, K. R. *J. Phys. Chem. Ref. Data* **1983**, *12*, 531.

(30) Wallington, T. J.; Hurley, M. D. *Chem. Phys. Lett.* **1992**, *193*, 84.

(31) (a) Howard, C. J. *J. Phys. Chem.* **1979**, *83*, 3. (b) Bird, R. B., Stewart, W. E., Lightfoot, E. N. *Transport Phenomena*; John Wiley and Sons: New York, 1960, 511.

(32) Brouard, M. Ph.D. Thesis, Oxford University, 1986.

(33) Frisch, M. J.; Trucks, G. W.; Schlegel, H. B.; Gill, P. M. W.; Johnson, B. G.; Robb, M. A.; Cheeseman, J. R.; Keith, T.; Petersson, G. A.; Montgomery, J. A.; Raghavachari, K.; Al-Laham, M. A.; Zakrzewski, V. G.; Ortiz, J. V.; Foresman, J. B.; Cioslowski, J.; Stefanov, B. B.; Nanayakkara, A.; Challacombe, M.; Peng, C. Y.; Ayala, P. Y.; Chen, W.; Wong, M. W. Andres, J. L.; Replogle, E. S.; Gomperts, R; Martin, R. L.; Fox, D. J.; Binkley, J. S., Defrees D. J. Baker, J.; Stewart, J. P.; Head-Gordon, M.; Conzales, C.; Pople, J. A. *Gaussian 94, Revision B.1*; Gaussian Inc.: Pittsburgh, PA, 1995.

(34) Westre, S. G.; Kelly P. B. *J. Chem. Phys.* **1989**, *90*, 6977.

(35) Sears, T. J.; Fyre. J. M.; Spriko, V.; Kraemer, W. P. *J. Chem. Phys.* **1989**, *90*, 2125.

(36) Jacox, M. E. *J. Phys. Chem. Ref. Data* **1984**, *13*, 945.

(37) Herzberg, G. *Molecular Spectra and Molecular Structure*; Van Nostrand: New York, 1945.

(38) Holbrook, K.; Pilling, M. J.; Robertson, S. H. *Unimolecular Reactions*; John Wiley: Chichester, 1996.

(39) Aubanel, E. E.; Wardlaw, D. M. *J. Phys. Chem.* **1989**, *93*, 3117.

(40) Hirst, D. M. *Chem. Phys. Lett.* **1985**, *122*, 225.

(41) Hase, W. L, Mondro, S. L.; Duchovic, R. J.; Hirst, D. M. *J. Am. Chem. Soc.* **1987**, *109*, 2917.

(42) Knyazev, V. D.; Benscura, A.; Dubinsky, I. A.; Gutman, D. *J. Phys. Chem.* **1995**, *99*, 14738.

(43) Hanning-Lee, M. L.; Green, N. J. B.; Robertson, S. H.; Pilling, M. J. *J. Phys. Chem.* **1993**, *97*, 860.

(44) Gang, J.; Pilling, M. J.; Robertson, S. H. *J. Chem. Soc., Faraday Trans.* **1997**, *93*, 1481.

(45) Davies, J. W.; Green, N. J. B; Pilling, M. J. *Chem. Phys. Lett.* **1986**, *126*, 373.

(46) Aubanel, E. E.; Robertson, S. H.; Wardlaw, D. M. *J. Chem. Soc., Faraday Trans.* **1991**, *87*, 2291.

(47) Brown, F. B.; Truhlar, D. G. *Chem. Phys Lett.* **1985**, *113*, 441.

(48) Schlegel, H. B. *J. Phys. Chem.* **1986**, *84*, 4530.

(49) Seakins, P. W.; Robertson, S. H.; Pilling, M. J.; Slagle, I. R.; Gmurczyk, G. W.; Benscura, A.; Gutman D. and Tsang, W. *J. Phys. Chem.* **1993**, *97*, 4450.

(50) Wardlaw, D. M.; Marcus, R. A. *Chem. Phys. Lett.* **1984**, *110*, 230.

(51) Wardlaw, D. M.; Marcus, R. A. *J. Chem. Phys.* **1985**, *83*, 3462.

(52) Wardlaw, D. M.; Marcus, R. A. *J. Phys. Chem.* **1986**, *90*, 5383.

(53) Wardlaw, D. M.; Marcus, R. A. *Adv. Chem. Phys.* **1988**, *70*, 231.

(54) Aston, J. G.; Eidenoff, M. L. *J. Chem. Phys.* **1935**, *3*, 379.

(55) Smith, S. C. *J. Phys. Chem.* **1993**, *97*, 7034.